

Review



Cite this article: Aidsburger M *et al.* 2021

Cold atoms meet lattice gauge theory. *Phil.*

Trans. R. Soc. A **380**: 20210064.

<https://doi.org/10.1098/rsta.2021.0064>

Received: 11 June 2021

Accepted: 23 August 2021

One contribution of 13 to a theme issue
'Quantum technologies in particle physics'.

Subject Areas:

atomic and molecular physics, gauge theory,
high-energy physics

Keywords:

quantum simulations, lattice gauge theory,
ultracold quantum matter

Author for correspondence:

Maciej Lewenstein

e-mail: maciej.lewenstein@icfo.eu

Cold atoms meet lattice gauge theory

Monika Aidsburger^{1,2}, Luca Barbiero^{3,4}, Alejandro Bermudez⁵, Titas Chanda^{6,7}, Alexandre Dauphin³, Daniel González-Cuadra³, Przemysław R. Grzybowski⁸, Simon Hands^{9,10}, Fred Jendrzejewski¹¹, Johannes Jünemann¹², Gediminas Juzeliūnas¹³, Valentin Kasper³, Angelo Piga^{3,14}, Shi-Ju Ran¹⁵, Matteo Rizzi^{16,17}, Germán Sierra¹⁸, Luca Tagliacozzo¹⁹, Emanuele Tirrito²⁰, Torsten V. Zache^{21,22}, Jakub Zakrzewski⁶, Erez Zohar²³ and Maciej Lewenstein^{3,24}

¹Fakultät für Physik, Ludwig-Maximilians-Universität München, Munich 80799, Germany

²Munich Center for Quantum Science and Technology (MCQST), München 80799, Germany

³ICFO—Institut de Ciències Fotoniques, The Barcelona Institute of Science and Technology, Castelldefels, Barcelona 08860, Spain

⁴Institute for Condensed Matter Physics and Complex Systems, DISAT, Politecnico di Torino, I-10129 Torino, Italy

⁵Departamento de Física Teórica, Universidad Complutense, Madrid 28040, Spain

⁶Institute of Theoretical Physics, Jagiellonian University in Kraków, Kraków 30-348, Poland


⁷The Abdus Salam International Centre for Theoretical Physics (ICTP), Strada Costiera 11, 34151 Trieste, Italy

⁸Institute of Spintronics and Quantum Information, Faculty of Physics, Adam Mickiewicz University in Poznań, Poznań, Poland

⁹Department of Physics, Faculty of Science and Engineering, Swansea University, Swansea SA28PP, UK

¹⁰Department of Mathematical Sciences, University of Liverpool, Liverpool L69 3BX, UK

- ¹¹Kirchhoff-Institut für Physik, Universität Heidelberg, Heidelberg 69120, Germany
- ¹²Institut für Physik, Johannes Gutenberg-Universität, Mainz 55128, Germany
- ¹³Institute of Theoretical Physics and Astronomy, Vilnius University, Vilnius 10257, Lithuania
- ¹⁴Departament de Chemical Engineering, Universitat Rovira I Virgili, 43007, Tarragona, Catalonia, Spain
- ¹⁵Department of Physics, Capital Normal University, Beijing 100048, People's Republic of China
- ¹⁶Forschungszentrum Jülich GmbH, Institute of Quantum Control, Peter Grünberg Institut (PGI-8), Jülich 52425, Germany
- ¹⁷Institute for Theoretical Physics, University of Cologne, Köln 50937, Germany
- ¹⁸Instituto de Física Teórica, UAM/CSIC, Universidad Autónoma de Madrid, Madrid, Spain
- ¹⁹Departament de Física Quàntica i Astrofísica and Institut de Ciències del Cosmos (ICCUB), Universitat de Barcelona, Barcelona, Catalonia 08028, Spain
- ²⁰International School for Advanced Studies (SISSA), Trieste 34136, Italy
- ²¹Center for Quantum Physics, University of Innsbruck, Innsbruck 6020, Austria
- ²²Institute for Quantum Optics and Quantum Information of the Austrian Academy of Sciences, Innsbruck 6020, Austria
- ²³Racah Institute of Physics, The Hebrew University of Jerusalem, Jerusalem 91904, Israel
- ²⁴ICREA, Passeig Lluís Companys 23, Barcelona 08010, Spain

 MA, 0000-0002-9476-3337; LB, 0000-0001-9023-5257; TC, 0000-0002-2306-7895; AD, 0000-0003-4996-2561; PRG, 0000-0003-2451-6776; SH, 0000-0001-5720-7852; GJ, 0000-0002-0677-6446; AP, 0000-0002-7409-2978; MR, 0000-0002-8283-1005; JZ, 0000-0003-0998-9460; EZ, 0000-0001-6993-6569; ML, 0000-0002-0210-7800

The central idea of this review is to consider quantum field theory models relevant for particle physics and replace the fermionic matter in these models by a bosonic one. This is mostly motivated by the fact that bosons are more ‘accessible’ and easier to manipulate for experimentalists, but this ‘substitution’ also leads to new physics and novel phenomena. It allows us to gain new information about among other things confinement and the dynamics of the deconfinement transition. We will thus consider bosons in dynamical lattices corresponding to the bosonic Schwinger or Z_2 Bose–Hubbard models. Another central idea of this review concerns atomic simulators of paradigmatic models of particle physics theory such as the Creutz–Hubbard ladder, or Gross–Neveu–Wilson and Wilson–Hubbard models. This article is not a general review of the rapidly growing field—it reviews activities related to quantum simulations for lattice field theories performed by the Quantum Optics Theory group at ICFO and their collaborators from 19 institutions all over the world. Finally, we will briefly describe our efforts to design experimentally friendly simulators of these and other models relevant for particle physics.

This article is part of the theme issue ‘Quantum technologies in particle physics’.

1. Introduction

Quantum simulators (QS) [1] constitute one of the pillars of quantum technology [2]. Although quantum advantage with QS was achieved many years ago [3], and keeps being repeated in various systems and contexts [4], most of the applications of QS concern quantum many-body physics. QS involve many platforms [5]: superconducting circuits [6], through ultracold atoms [7], trapped ions [8], Rydberg atoms [9], circuit QED [10], photonic systems [11] and more. QS has enriched our understanding of quantum many-body systems in the last decades enormously: from the physics of Fermi–Hubbard models [12] to non-trivial aspects of interacting disordered systems and many-body localization [13].

Typically, QS are thought to mimic condensed matter physics, but as early as 2005 people started to talk about simulations of high energy physics and, in particular, lattice gauge theories (LGTs) [14,15]. Several proposals/designs were later formulated, employing typically quantum link models [16] in which gauge fields are represented on the links of the lattice in a finite-dimensional Hilbert space (see for instance [17–22]). These designs can often be analysed efficiently in terms of tensor networks methods (TN)—a European collaboration programme QTFLAG made essential progress in this respect (for a review see [23]). Amazingly, many of these theoretical designs were reformulated in an ‘experiment-friendly’ manner, and have found experimental realizations, or at least ‘first-experimental-steps-toward-realization’ [24–28].

As an example of such LGT design consider a toolbox for LGTs [29] where a class of simple two-dimensional models admitting a low energy description in terms of an Abelian gauge theory is proposed. The models display rich phase diagrams, with exotic deconfined phases and gapless phases—a rare situation for two-dimensional Abelian gauge theories emerging from the additional symmetry in these models. Shaken ultracold bosonic atoms in optical lattices provide a possible experimental platform for this toolbox proposal.

The present paper for this special issue reviews activities in the field of QS of LGTs and related models performed by the Quantum Optics Theory group at ICFO in collaboration with many others. It has a review character, but includes also some novel, unpublished results.

We would like to stress that we, and many of our colleagues working in particle and nuclear physics, believe that theoretical and experimental studies of models review here enriches our understanding of quantum many-body physics in general, and particle and nuclear physics in particular. For instance, as our referee points out: ‘It is very interesting to consider models like the Z_2 Bose-Hubbard model, with the consequent new physical phenomena and phases. However, from the particle physics perspective, these new aspects somehow turn the attention away from the key mechanisms of interest in particle physics’. Obviously, the core particle physics community would be interested in ‘pure’ models better-known to the community. The ‘holy grail’ that probably most of us would like to see would be a quantum simulation of QCD, to address non-zero matter density and/or real-time dynamics. While it is clear quantum simulations are not yet at this stage, it would be very welcome to address simpler models, but not necessarily ones with phenomena exotic to particle physicists. As our referee points out: ‘This could be done by isolating some limits of the generalized models, i.e. limits that correspond to the standard models of particle physics, e.g. pure Z_2 without the Bose-Hubbard overhead. From the point of view of experimental realization, unfortunately, simpler models might not necessarily be simpler to realize’. We must admit that we are just at the beginning of the ‘long and winding road’, and the quest for ‘pure’ models, relevant directly to particle and nuclear physics, has just started and is intensively pursued.

Section 2 presents recent achievements in the physics of the bosonic Schwinger model. Characteristically for cold atoms, experiments are much easier for bosons motivating this work which parallels the more extensively studied fermionic case. Section 3 describes bosons on lattices in a tight-binding approach via the Bose–Hubbard model, but with tunnellings mediated by other atomic species with certain symmetries. Section 4 deals with Creutz–Hubbard and Creutz–Ising ladders as well as the paradigmatic Gross–Neveu–Wilson and Wilson–Hubbard models. Last but not least, §5 discusses dynamical gauge field simulators that are the most experimentally friendly. We discuss future perspectives and conclude in §6.

2. Bosonic Schwinger model

The renowned fermionic Schwinger model (FSM) [30,31] describes one of the simplest gauge theories in $1 + 1$ dimensions: it has been studied extensively over the years [32–36] as it enjoys interesting features similar to quantum chromodynamics (QCD) in $3 + 1$ dimensions, such as a confinement and a breaking of chiral symmetry (that in the Schwinger model occurs via an anomaly). In this section, we consider its far less-explored bosonic counterpart, the bosonic Schwinger model (BSM) [37] that also manifests strong confinement phenomena.

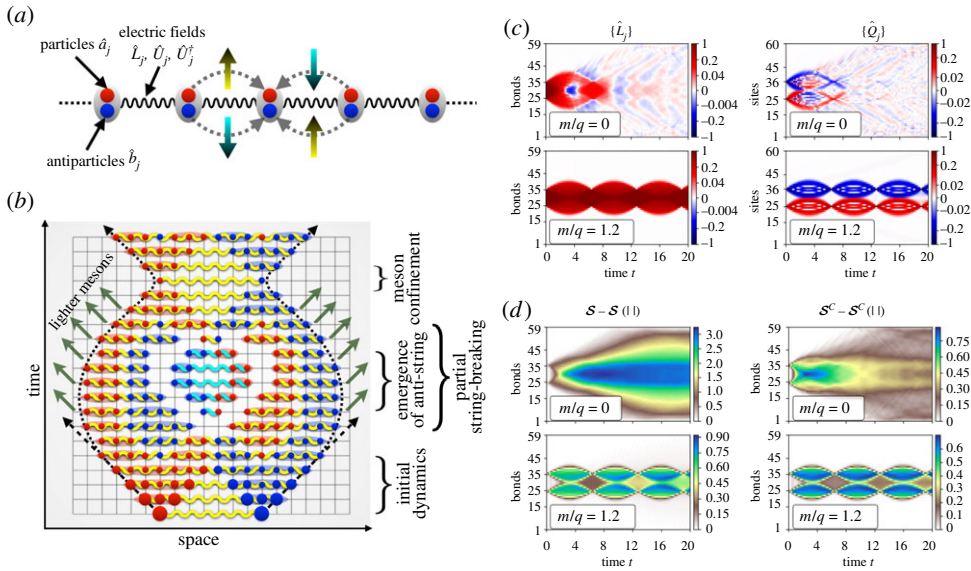


Figure 1. The bosonic Schwinger model and its time-evolution [37]: (a) schematic depiction of BSM, where lattice sites are populated by particles (red circles) and antiparticles (blue circles) and the bonds between neighbouring sites hold U(1) electric gauge fields. Left moving particles (antiparticles) raise (lower) the quantum state of the electric field in a corresponding bond, while the opposite holds for right moving bosons. (b) Sketch of the confining dynamics of BSM. The system is driven out of equilibrium by creating spatially separated particle–antiparticle pair connected by a string of electric field (a yellow wiggly line). The strong confinement of bosons bends the trajectory of both excitations. New dynamical charges are created during the evolution that partially screen the electric field. However, the electric field oscillates coherently and may form an anti-string (cyan wiggly line), creating a central core of strongly correlated bosons that is very different from an equilibrium state. This strange central region survives despite the fact that the boson density in the central region may be depleted through the radiation of lighter mesons that can propagate freely. (c) Dynamics of the electric field $\langle \hat{L}_j \rangle$ and the dynamical charge $\langle \hat{Q}_j \rangle$, and (d) the same for the total entanglement entropy \mathcal{S} measured across different bonds and its classical part \mathcal{S}^C . (Online version in colour.)

The BSM is described by relativistic scalar bosons coupled to an U(1) gauge field in one dimension. The discretized Hamiltonian of the BSM is given by (see [37] for details)

$$\begin{aligned} \hat{H} = & \sum_j \hat{L}_j^2 + 2 \left(x \left(\left(\frac{m}{q} \right)^2 + 2x \right) \right)^{1/2} \sum_j (\hat{a}_j^\dagger \hat{a}_j + \hat{b}_j \hat{b}_j^\dagger) \\ & - \frac{x^{3/2}}{((m/q)^2 + 2x)^{1/2}} \sum_j [(\hat{a}_{j+1}^\dagger + \hat{b}_{j+1}) \hat{U}_j (\hat{a}_j + \hat{b}_j^\dagger) + \text{H.c.}], \end{aligned} \quad (2.1)$$

where q is the electric charge, m the bare mass of particles, x is related to the discrete lattice-spacing a by the relation $x = 1/(a^2 q^2)$, $\{\hat{a}_j^\dagger, \hat{a}_j\}$, $\{\hat{b}_j^\dagger, \hat{b}_j\}$ are bosonic creation-annihilation operators corresponding to particles and antiparticles, respectively, and \hat{L}_j the electric field operator residing on the bond between sites j and $j+1$ with $\{\hat{U}_j, \hat{U}_j^\dagger\}$ being U(1) ladder operators satisfying $[\hat{L}_j, \hat{U}_l] = -\hat{U}_j \delta_{jl}$ and $[\hat{L}_j, \hat{U}_j^\dagger] = \hat{U}_j^\dagger \delta_{jl}$. The system is presented schematically in figure 1a.

The Hamiltonian is invariant under local U(1) transformations: $\hat{a}_j \rightarrow e^{i\alpha_j} \hat{a}_j$, $\hat{b}_j \rightarrow e^{-i\alpha_j} \hat{b}_j$, $\hat{U}_j \rightarrow e^{-i\alpha_j} \hat{U}_j e^{i\alpha_{j+1}}$, where the corresponding Gauss Law generators are given by $\hat{G}_j = \hat{L}_j - \hat{L}_{j-1} - \hat{Q}_j$, with $\hat{Q}_j = \hat{a}_j^\dagger \hat{a}_j - \hat{b}_j^\dagger \hat{b}_j$ being the dynamical charge. We consider the physical subspace spanned by the set of states, $|\Psi\rangle$ that are annihilated by \hat{G}_j . The low energy spectrum of this system is always gapped even for massless bosons, and as a result the bosons are always confined [37]. As

an example we review, here, the strong confining dynamics of the system of finite size N using matrix-product-state (MPS) techniques [38–40].

The out-of-equilibrium dynamics (OED) of the BSM is initiated by creating two extra dynamical charges of opposite signs, at positions $N/2 - R$ and $N/2 + R + 1$, respectively, connected by a string of electric field on top of the ground state $|\Omega\rangle$ by the non-local operator $\hat{M}_R \equiv (\hat{a}_{N/2-R}^\dagger + \hat{b}_{(N/2)-R})[\prod_{j=(N/2)-R}^{(N/2)+R} \hat{U}_j^\dagger](\hat{a}_{(N/2)+R+1} + \hat{b}_{(N/2)+R+1}^\dagger)$. In an ergodic system, two such excess particles would rapidly delocalize and the system would return to a state indistinguishable from equilibrium. Here we observe something very different as described in the cartoon of the dynamics in figure 1b: (i) the light cone of the excitations always bends, representing a slowing down and inversion of their trajectories, as a result of the strong confinement; (ii) the initial extended meson formed by the two charges and the electric-flux string connecting them is very robust and the string of electric field joining the two excitations does not break, but rather undergoes at least a couple of coherent oscillations; (iii) for lighter masses, we observe a string-inversion phenomenon and radiation of lighter mesons from the central region; (iv) even once the radiated mesons are free to escape from the confined region and fly away with a constant velocity, as expected in ergodic systems, they leave behind a strongly correlated central core where bosons are confined. The footprints of these phenomena are presented in figure 1c by considering spatio-temporal profiles of the electric field $\langle \hat{L}_j \rangle$ and the dynamical charge $\langle \hat{Q}_j \rangle$ for two values of bare mass $m/q = 0$ and 1.2, that together display all the phenomena listed above. For the massless case, due to a meson radiation from the edges, the confined core of bosons is gradually depleted and disappears after a finite time ($t \approx 10$), while for $m/q = 1.2$ both gauge and particle sectors show long-lived coherent oscillations.

In order to better understand the nature of the ergodicity violation, we consider the dynamics of the bond-resolved entanglement entropy S_j , measured across the bond between the sites j and $j + 1$, presented in the left column of figure 1d. For $m/q = 0$ most of the entanglement is contained in the central confined region and persists even long after the concentration of bosons in the bulk disappears at around $t \approx 10$, showing a strong memory effect and hence a lack of thermalization. As a result of the U(1) symmetry related to the conservation of the total charge $\sum_j \hat{Q}_j$, the reduced density matrices of the system are block-diagonal. There are two contributions to the entanglement entropy [41,42] $S = S^C + S^Q$, a classical part (the Shannon entropy between different quantum sectors), and a quantum part. While the quantum part S^Q qualitatively follows the pattern of total entropy S , the classical part S^C shows strong non-ergodic behaviour by sharply demarcating confined and deconfined domains as depicted in the right column of figure 1d. Summarizing, the strong spatial inhomogeneity of the time-evolved entropies, especially of their classical part, gives us a clear generic signature of the persistent memory effect and lack-of-thermalization and ergodicity in the system.

For detailed analysis of such non-ergodic behaviour in BSM by means of entropy scaling, we refer the reader to [37]. Specifically, it was shown that the central confined region remains non-thermal, while the external deconfined region seems to thermalize—thus producing exotic asymptotic states.

3. Strongly correlated bosons on a dynamical lattice

Fermionic matter coupled to dynamical gauge fields has been more extensively explored than its bosonic counterpart, mainly due to the fermionic nature of the matter sector in the Standard Model of particle physics. As presented in the last section, much of the relevant high-energy phenomenology is also present in LGTs with bosonic matter, additionally showing novel strongly correlated effects. These could be further explored using ultracold atoms in optical lattices, with the additional benefit that bosonic atoms are easier to control experimentally. In §5, we will present realistic experimental proposals as well as review the current experimental status to simulate LGTs with cold atoms.

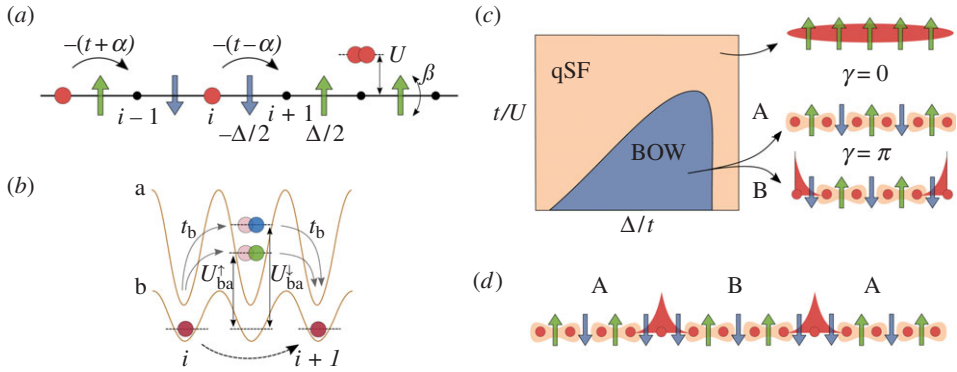


Figure 2. Symmetry-breaking topological insulators [46]: (a) sketch of the \mathbb{Z}_2 BHM (3.3). Bosonic particles (red spheres) hop on a one-dimensional lattice interacting among themselves and with \mathbb{Z}_2 fields (arrows). The latter are located on lattice links and their configuration modifies the tunnelling strength. (b) The model describes a mixture of ultracold bosonic atoms in an optical lattice, where two hyperfine states of one deeply trapped species (green/blue spheres) simulates the \mathbb{Z}_2 field [45]. The correlated tunnelling term can be obtained as a second-order density-dependent tunnelling process of the other species [47]. (c) Qualitative phase diagram at half filling. For strong enough Hubbard interactions, the system undergoes a bosonic Peierls transition from a qSF to a BOW phase where the field orders anti-ferromagnetically [48]. The two degenerate symmetry-broken patterns (A and B) give rise to insulating states, one of which manifests non-trivial topological properties such as localized edge states with a fractional bosonic number. (d) The presence of dynamical fields and the interplay between symmetry breaking and topological symmetry protection gives rise to strongly correlated effects that are absent in a static lattice. In the figure, topological defects are shown between the different symmetry-broken field patterns, hosting fractional bosonic states that can move along the system's bulk [46,49]. (Online version in colour.)

In this section, we will explore a further simplification that also leads to interesting phenomena in related models. We start from the simplest LGT with dynamical matter, i.e. a one-dimensional chain of bosons coupled to a \mathbb{Z}_2 gauge field [43],

$$H_{L_2} = -\alpha \sum_i (b_i^\dagger \sigma_{i,i+1}^z b_{i+1} + \text{H.c.}) + \beta \sum_i \sigma_{i,i+1}^x, \quad (3.1)$$

Although a quantum simulation of the full one-dimensional chain is still lacking, the minimal building block of this model, a gauge-invariant correlated tunnelling term, has already been implemented with ultracold atoms using Floquet engineering [25]. This technique uses fast periodic driving of a given system leading to an effective time-averaged Hamiltonian of hopefully desired properties. We now consider adding extra terms to the Hamiltonian that break gauge invariance. In particular, we include the standard Bose–Hubbard Hamiltonian describing ultracold bosonic atoms in optical lattices [44],

$$H_{\text{BH}} = -t \sum_i (b_i^\dagger b_{i+1} + \text{H.c.}) + \frac{U}{2} \sum_i n_i(n_i - 1), \quad (3.2)$$

as well as a parallel field for the gauge degrees of freedom, $H_\Delta = (\Delta/2) \sum_i \sigma_{i,i+1}^z$. We denote the full Hamiltonian as the \mathbb{Z}_2 Bose–Hubbard model (\mathbb{Z}_2 BHM) [45]

$$H_{L_2\text{BH}} = H_{L_2} + H_{\text{BH}} + H_\Delta, \quad (3.3)$$

describing a chain of strongly correlated bosons whose tunnelling elements depend locally on the \mathbb{Z}_2 field configuration (figure 2a).

The \mathbb{Z}_2 BHM could be implemented more easily in cold-atom experiments than the \mathbb{Z}_2 LGT (3.1), as it does not require the complete elimination of bare bosonic tunnelling. Both this and the correlated tunnelling term can be obtained as second-order processes in ultracold bosonic mixtures (figure 2b). In particular, the ratio between these two terms can be controlled

experimentally using a Feshbach resonance [47], with

$$\frac{\alpha}{t} = \frac{(U_{ba}^{\downarrow} - U_{ba}^{\uparrow})}{(U_{ba}^{\downarrow} + U_{ba}^{\uparrow})}, \quad (3.4)$$

where U_{ba}^{σ} denotes the interspecies Hubbard interactions and $\sigma = \uparrow, \downarrow$ is the internal hyperfine state of one species, simulating the field degrees of freedom.

The \mathbb{Z}_2 BHM also resembles the Su–Schrieffer–Heeger (SSH) model [50], with the \mathbb{Z}_2 field playing the role of phonons in solid-state systems. The former can thus be understood as simplified lattice degrees of freedom, allowing to simulate a dynamical lattice using ultracold atoms that otherwise are subjected to a static optical potential [7]. Similarly to the SSH model, the \mathbb{Z}_2 BHM also presents Peierls instabilities [51], even in the absence of a Fermi surface, giving rise to Bond Order Wave (BOW) phases where the field develop long-range order (figure 2c) [45]. At half filling, the spontaneous symmetry breaking (SSB) of translational invariance gives rise to two degenerate ground states characterized by a dimerized tunnelling pattern. Although both states share the same symmetry properties, they can be distinguished using a topological invariant such as the Berry phase γ [52], quantized to 0 or π in the presence of inversion symmetry. A value of $\gamma = \pi$ corresponds to non-trivial bulk topology, also signalled by the presence of localized states at the system’s boundary carrying fractional particle number (figure 2c).

The topological Peierls insulators with BOW order found in the \mathbb{Z}_2 BHM are thus examples of interaction-induced symmetry-breaking topological phases. The interplay between long-range order and non-trivial topology gives rise to strongly correlated effects that are absent in topological phases where SSB does not take place. For instance, upon doping the system above half filling, the ground state presents topological defects that separate the two symmetry-broken degenerate configurations (figure 2d). Each of these defects separates regions with different bulk topology, hosting localized fractional states [46,49]. These are similar to the edge states found at the boundary, but in this case the defect-fractional boson composite quasi-particle can move within the system’s bulk, contributing to its transport properties.

Still richer phenomenology can be found at other fractional values of the bosonic density. At $\rho = 1/3$ and $\rho = 2/3$, the Peierls instability gives rise to BOW order with a three-site unit cell (figure 3a). Among all the possible configurations, only two present inversion symmetry, protecting non-trivial topological properties. Remarkably, such configurations appear in the ground states for certain values of the Hubbard interaction [53]. We observe, in particular, an interaction-induced topological phase transition where the protecting symmetry is first spontaneously broken in an intermediate phase and then emerges again (figure 3a). The mechanism behind this process is related to the Peierls constraint: for these values of the bosonic density it is energetically favourable to keep a three-site unit cell. A direct topological transition between the two inversion-symmetric patterns would go through a point where translational invariance is restored. Instead, it is more favourable to break inversion symmetry in an intermediate region to also keep translational invariance broken.

Such symmetry-constrained topological phase transitions are again a consequence of the interplay between SSB and topology. Furthermore, they can be used to devise a self-adjusted fractional pumping mechanism [54]. A pumping protocol is a periodic adiabatic modulation where the system’s ground state follows a trajectory in parameter space encircling a critical point, transporting in the process a quantized number of particles. If the critical point is topological, this value will be non-zero, and can be computed in terms of a topological invariant. This process normally requires the protecting symmetry to be explicitly broken. In our case, this happens spontaneously just by modifying the Hubbard interactions. Adding an extra field to break the ground state degeneracy and to choose the degenerate configuration to which the system transitions, we can create a protocol that encircles the critical point and go through all degenerate trivial and topological configurations (figure 3b). The cycle can be divided in three and the particle number transported in each of them is topologically quantized to the fractional value $1/3$.

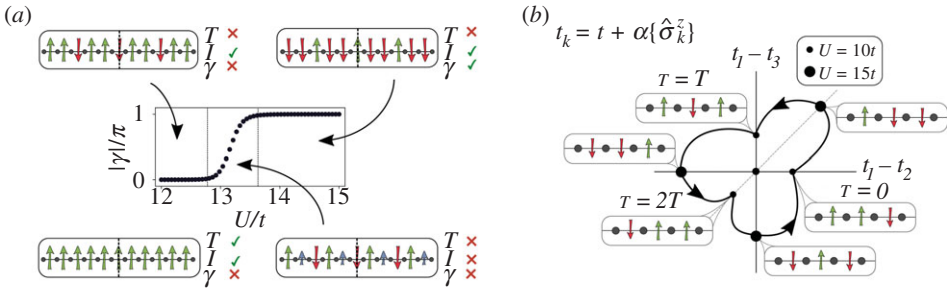


Figure 3. Emergent symmetry protection and fractional pumping [53]. (a) For fractional densities other than half filling, the SSB of translational invariance (T) can also break the protecting inversion symmetry (I). For $\rho = 1/3$ and $\rho = 2/3$, the latter emerges again for sufficiently strong values of U , giving rise to non-trivial topology ($\gamma = \pi$) while maintaining a trimmerized pattern along the phase transition [53]. (b) Such a symmetry-constrained transition can be employed to devise a self-adjusted pumping protocol, where the system travels adiabatically along the trivial and topological (threefold) degenerate configurations. Each trivial–topological–trivial subcycle transport $1/3$ of a boson [53]. In the figure, $\langle \hat{\sigma}_k^z \rangle$, with $k = 1, 2, 3$ denotes the expectation value of the field within the repeating unit cell. (Online version in colour.)

In this section, we have discussed the topological properties of the \mathbb{Z}_2 BHM for some specific densities. Peierls instabilities, however, can occur *a priori* for any density. It turns out that this is also the case here, where a staircase of topological Peierls insulators is found in the phase diagram, together with regions where incommensurate orders develop, giving rise to Peierls supersolids [47]. The above results indicate how ultracold atoms in optical lattices can be used to explore interested strongly correlated phenomena inspired, but not restricted to, those appearing in condensed matter and high-energy physics.

4. The synthetic Creutz–Hubbard model

Understanding the robustness of topological phases of matter in the presence of interactions poses a difficult challenge in modern condensed matter, showing interesting connections with high-energy physics. An example lies in the physics of topological insulators, which are insulating phases of matter that are not characterized by local order parameters but, instead, by certain topological invariants [55]. Some of these correlated topological insulators such as *Wilson–Hubbard topological matter* can be described in terms of a relativistic quantum field theory (QFT) of massive Wilson fermions with four-Fermi interactions [56], which originally appeared in the context of lattice gauge theories for elementary particle physics [57]. The precursors of this physics were already discussed for non-interacting models and static gauge fields [58,59].

Creutz–Hubbard model: Here we will focus on the Creutz topological insulator [60] and its connection with the Gross–Neveu–Wilson model [61]. In particular we will consider the imbalanced Creutz model [62] consisting of spinless fermions on a two-leg ladder. These fermions are created and annihilated by $c_{j,l}^\dagger, c_{j,l}$ where $j \in \{1, \dots, N\}$ labels the lattice sites within the upper or lower legs $l \in \{u, d\}$ and evolve according to the tight-binding Hamiltonian

$$H_C = \sum_{jl} \left(-t_l c_{j+1,l}^\dagger c_{j,l} - t_x c_{j+1,l}^\dagger c_{j,\bar{l}} + \frac{\Delta \epsilon_l}{4} c_{j,l}^\dagger c_{j,l} + \text{H.c.} \right). \quad (4.1)$$

Here, $t_l = t e^{-i\pi s_l/2}$ represents the horizontal hopping strength dressed by magnetic π -flux, t_x stands for the diagonal hopping, $\Delta \epsilon_l = \Delta \epsilon s_l$ with $\Delta \epsilon > 0$ is a energy imbalance between the legs of the ladder, and we use the notation $s_u = 1$ ($s_d = -1$) and $\bar{l} = d$ ($\bar{l} = u$) for $l = u$ ($l = d$). We now consider the addition of a quartic interaction term to the Hamiltonian

$$H_v = \frac{V_v}{2} \sum_{j,l} c_{j,l}^\dagger c_{j,l}^\dagger c_{j,\bar{l}} c_{j,\bar{l}}, \quad (4.2)$$

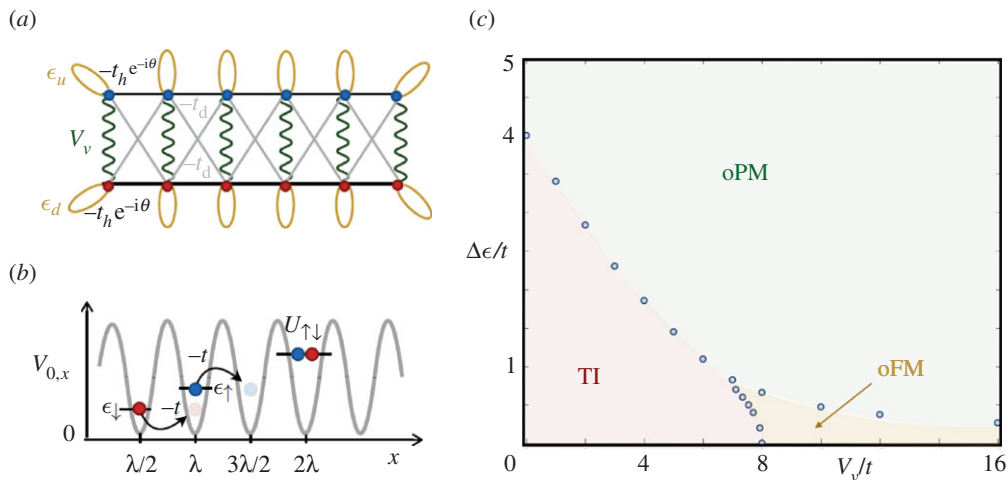


Figure 4. Creutz topological insulator: (a) the imbalanced Creutz ladder defined in equation (4.3) in the π -flux limit. (b) Atoms in two hyperfine states $|\uparrow\rangle, |\downarrow\rangle$ are trapped at the minima of an optical lattice. At low temperatures, the kinetic energy of the atoms can be described as a tunnelling of strength $-t$ between the lowest energy levels $\epsilon_{\uparrow}, \epsilon_{\downarrow}$ of neighbouring potential wells. Additionally, the s -wave scattering of the atoms leads to contact interactions of strength $U_{\uparrow\downarrow}$ whenever two fermionic atoms with different internal states meet on the same potential well. (c) Phase diagram of the C–H model. It displays a topological insulator phase (TI), and two other non-topological phases, namely an orbital phase with long-range ferromagnetic Ising order (oFM), and an orbital paramagnetic phase (oPM). The blue circles label numerical results and the coloured phase boundaries are a guide to the eye. (Online version in colour.)

and denote the full Hamiltonian as the imbalanced Creutz–Hubbard Hamiltonian

$$H_{CH} = H_C + H_V, \quad (4.3)$$

describing a ladder of strongly correlated fermions whose tunnelling and interactions are depicted in figure 4a.

The Creutz–Hubbard model could be implemented with ultra-cold fermions in intensity-modulated optical lattices. Moreover, this model represents a workhorse in the study of strongly correlated topological phases in the so-called synthetic quantum matter in atomic, molecular and optical (AMO) platforms, more particularly, with ultracold gases of neutral atoms in optical lattices (figure 4b). Indeed, two accessible AMO ingredients, such as (i) a simple Zeeman shift between the atomic internal states, and (ii) Feshbach resonances, lead to a leg imbalance enabling tuning of the Hubbard-type interaction in the ladder.

The model has an interesting phase diagram shown in figure 4c. In the non-interacting regime, we can rewrite the Hamiltonian H_C in momentum space as $H_C = \int_{-\pi}^{\pi} \Psi^\dagger(k) h_C(k) \Psi(k)$ with the single particle Hamiltonian

$$h_C(k) = -2t_x \sigma^x \cos k + \left(\frac{1}{2} \Delta\epsilon + 2t \sin k\right) \sigma^z. \quad (4.4)$$

This single-particle Hamiltonian respects the sub-lattice symmetry S : $U_S h_C(k) U_S^\dagger = -h_S(k)$ but breaks both time-reversal and particle-hole symmetries. For this reason, the imbalanced Creutz model yields a symmetry-protected topological phase in the AIII class [63]. For $\Delta\epsilon = 0$, one finds that the system develops two topological flat bands. This flat bands have an associated topological invariant that can be defined through the Berry connection $\mathcal{A}_\pm(k) = i\langle\epsilon_\pm(k)|\partial_k|\epsilon_\pm(k)\rangle = 1/2$. The uniform Berry connection leads to a finite Zak’s phase [64] as $\phi_{Zak,\pm} = \int dq \mathcal{A}_\pm(q)$ and equals $\phi_{Zak,\pm} = \pi$. Switching on the leg imbalance $\Delta\epsilon > 0$ leads to some curvature in energy bands. The Berry connection becomes non-uniform and depends on the band curvature $\phi_{Zak,\pm} = \pi\theta(f-1)$ (where $f = 4t/\Delta\epsilon$ is the curvature). Hence Zak’s phase yields a topological effect until $f > 1$, i.e.

$\Delta\epsilon < 4t$. For $f < 1$ ($\Delta\epsilon > 4t$), the band curvature is large and no topological phenomena occur. This marks a quantum phase transition between the AIII topological insulator and a trivial band insulator as shown along the vertical axis as figure 4c. Moreover, turning on interactions leads to a competition between topological phases and two different phases of orbital magnetism. As shown in figure 4c, at large interaction strength a long-range in-plane ferromagnetic order arises, related to the symmetry-broken phase of an orbital quantum Ising model, while the Zeeman imbalance then drives a standard quantum phase transition in the Ising universality class towards an orbital paramagnetic phase. Recently, it has been pointed out that the so-called mean chiral displacement, an observable readily available in after-quench dynamical experiments, could provide a faithful readout of such tripartite phase diagram [65]. On top of that—similarly to what was observed for Peierls insulators in §3—a staircase of gapped phases emerges at fractional filling fractions and exhibits (symmetry protected) topological signatures [66]. Finally, in [67], the static flux was promoted to a dynamical variable, converting the Creutz model into a lattice gauge theories where different mechanism to obtain both topological order and fermionic deconfinement were unveiled in the absence of a plaquette term.

Wilson–Hubbard model: In the thermodynamic limit, the rungs of the ladder play the role of the one dimensional Bravais lattice $ja \rightarrow x \in \Lambda_l = aZ^d = \{x : x_i \in Z, \forall i = 1, \dots, d\}$, while the ladder index $l \in \{u, d\}$ plays the role of the spinor degrees of freedom of the Fermi field $\Psi(x) = (c_{j,u}, c_{j,d})^t$. Making a gauge transformation $c_{j,l} \rightarrow e^{i\pi j/2} c_{j,l}$, one find that the above imbalanced Creutz model (4.1) can be rewritten as a *one-dimensional Wilson-fermion Hamiltonian* lattice field theory (LFT). In general, the Wilson LFT is defined by the following Hamiltonian:

$$\begin{aligned} \mathcal{H}_W = \sum_{x \in \Lambda_l} [\Psi^\dagger(x) \left(\frac{i\alpha_i}{2} + \frac{\delta m_i \beta}{2} \right) \Psi(x + au^i) + m \Psi^\dagger(x) \frac{\beta}{2} \Psi(x) + \text{H.c.}] \\ + \sum_{\nu\mu} \sum_{x \in \Lambda_l} \Psi_\mu^\dagger(x) \Psi_\nu^\dagger(x) \frac{u_{\mu\nu}}{2} \Psi_\mu(x) \Psi_\nu(x) \end{aligned} \quad (4.5)$$

where the parameters δm_i quantify a certain mass shift introduced to put the fermion doublers up to the cut-off scale of the LFT, and $u_{\mu,\nu} = (1 - \delta_{\mu,\nu})g^2$ encode the interaction strengths. In the long-wavelength approximation, the Wilson-fermion LFT yields a continuum Wilson-fermion QFT for N_D instances of the massive Dirac QFT, each describing a relativistic fermion with a different Wilson mass m_n and single-particle Hamiltonian $h^n(k) = \alpha_i^n k^i + m_n \beta$. In the case of the Creutz model, the Wilson LFT is found by making the following identification of Dirac matrices $\alpha = \sigma^x$, $\beta = \sigma^z$; it describes $N_D = 2$ Wilson fermions. Moreover, from the perspective of topological insulators, the topological invariants are non-local quantities and thus also sensitive to the Wilson fermion masses. Indeed for the Chern characters Ch_1 or Chern–Simons forms CS_1 [68] we have that $\text{Ch}_1 = \frac{1}{2} \sum_n p_n \text{sign}(m_n)$ and $\text{CS}_1 = \frac{1}{4} \sum_n p_n \text{sign}(m_n)$ [69]. This means that if the lattice parameters δm_i are chosen such that a mass inversion occurs for some of the Wilson fermions, it becomes possible to obtain a non-vanishing integer-valued topological invariant.

Gross–Neveu–Wilson model: It is possible to map the imbalanced Creutz–Hubbard ladder to a discretized version of the Gross–Neveu field theory: the Gross–Neveu–Wilson field theory. This QFT describes Dirac fermions with N flavours interacting via quartic coupling which live in one spatial and one time dimension. In the continuum, the model is described by the following normal-ordered Hamiltonian $H = \int dx : \mathcal{H} :$ with

$$\mathcal{H} = -\bar{\Psi}(x) i \gamma^1 \partial_x \Psi(x) - \frac{g^2}{2N} (\bar{\Psi}(x) \Psi(x))^2. \quad (4.6)$$

Here $\bar{\Psi}(x) = (\bar{\Psi}_1(x), \dots, \bar{\Psi}_N(x))$ where $\bar{\Psi}_n(x) = \Psi_n^\dagger(x) \gamma^0$ are two-component spinor field operators for the n th fermionic species, and $\gamma^0 = \sigma^z$, $\gamma^1 = i\sigma^y$ are the gamma matrices, which can be expressed in terms of Pauli matrices for $(1+1)$ -dimensional Minkowski space-time, leading to the chiral matrix $\gamma^5 = \gamma^0 \gamma^1 = \sigma^x$. Therefore, the Gross–Neveu model describes a collection of N copies of massless Dirac field coupled via quartic interactions. According to the above discussion and using the exact relations $ma = (\Delta\epsilon/4t) - 1$ and $g^2 = (V_v/2t)$, the Wilsonian discretization of

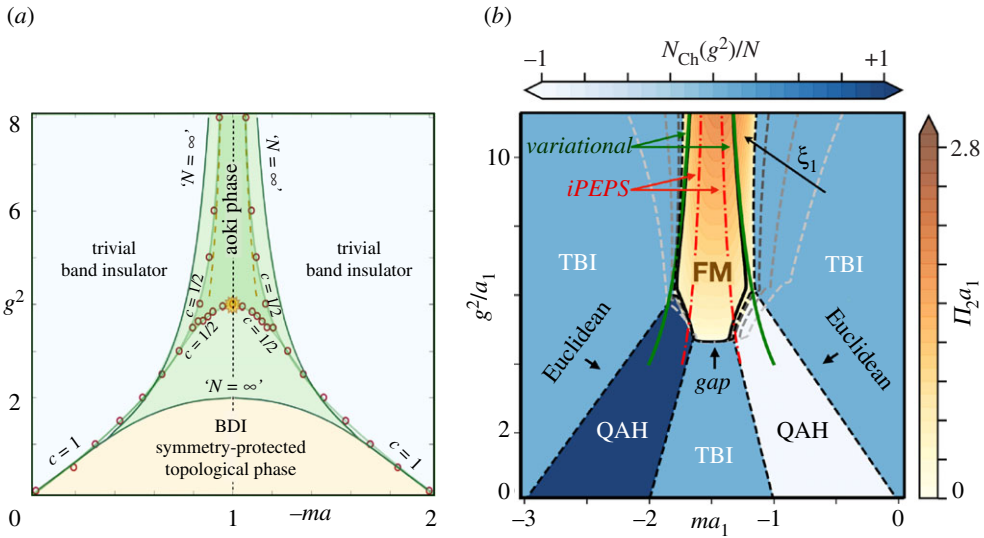


Figure 5. Gross–Neveu model phase diagrams: (a) Phase diagram of $(1+1)d$ Gross–Neveu model. The two green solid lines correspond to the critical lines found by large- N techniques. Red circles represent the critical points of the $N=1$ Gross-Neveu lattice model obtained with MPS. The semi-transparent green lines joining these points delimit the trivial band insulator, Aoki phase, and the BDI symmetry-protected topological phase. We also include the exact critical point at $(-ma, g^2) = (1, 4)$, which is depicted by an orange star, and the strong-coupling critical lines that become exact in the limit of $g^2 \rightarrow \infty$, depicted by dashed orange lines. MPS predictions match these exact results remarkably well. (b) Phase diagram of $(2+1)d$ Gross–Neveu model. Contour plots of the Chern number N_{Ch} (blue) and π condensate (orange), predicting large- N QAH phases, trivial band insulators (TBIs) and a ferromagnetic phase (FM). The black solid line is obtained by solving self-consistent equations (Gap), which can delimit the area of the FM, but give no further information about the TBI or QAH phases. The green solid lines (variational) represent the product-state prediction for the compass model, and the red dashed-dotted lines correspond to iPEPs. (Online version in colour.)

the Gross–Neveu QFT on a uniform lattice (defined in equation (4.5)) is gauge-equivalent to the imbalanced Creutz–Hubbard model of condensed-matter physics [70]. Figure 5a shows the phase diagram of the model. We have applied large- N techniques borrowed from high-energy physics, complemented with the study of topological invariants from condensed matter, to unveil a rich phase diagram that contains a wide region hosting a BDI topological insulator. This region extends to appreciable interaction strength g^2 , and thus corresponds to a strongly correlated symmetry-protected topological phase. Moreover, for sufficiently strong interactions, a gapped phase where parity symmetry is spontaneously broken, *viz.* the Aoki phase, is formed due to the appearance of a pseudoscalar fermion condensate $\Pi \propto \langle \bar{\psi} i \gamma^5 \psi \rangle$. The large- N prediction has allowed us to find the critical line separating the topological insulator from the Aoki phase by studying the onset of the pseudoscalar condensate, and show that it terminates at tricritical point where all three phases of matter coexist.

The model can easily be extended to $(2+1)$ dimensions [71]. In figure 5b, we show the complete phase diagram of the model together with the contour plot of the Chern number and the pseudo-scalar condensate. In the non-interacting regime $g^2 \approx 0$, the single-flavour $(2+1)d$ Gross–Neveu–Wilson model corresponds to the square-lattice version [72] of the Haldane model [73] of the quantum anomalous Hall effect (QAH). This model has a quantized Hall conductance $\sigma_{xy} = (e^2/h)N_{Ch}$ with $N_{Ch} = (N/2) \sum_{n_d} (-1)^{(n_{d,1}+n_{d,2})} \text{sign}(m_{n_d})$. With the interaction switched on the fermions can also form polar condensates $\Pi_1 \propto \langle \bar{\psi} \gamma^1 \psi \rangle$ and $\Pi_2 \propto \langle \bar{\psi} \gamma^2 \psi \rangle$ related to the spontaneous breaking of parity symmetry and Lorentz-invariance. The set of parameters where the Π condensates form define critical line separating the correlated QAH phase from long-range-ordered ferromagnets as depicted in figure 5b.

5. Experimental and experimentally friendly quantum simulators

Spectacular advances in the field of artificial quantum systems make it possible to realize lattice gauge theories with quantum simulators in table-top experiments. Platforms that succeeded in achieving this goal so far are trapped ions [24,74], ultracold atoms [25–28] and superconducting qubits [75]. A common characteristic shared by these experimental platforms is their high tunability and precise readout, which provides a toolbox distinct from those of particle physics or solid-state experiments. For example, quantum simulators allow for a tuning of the microscopic parameters, studying isolated quantum many-particle dynamics in real time, or measuring higher-order correlations [76,77] and entanglement [78].

In the following, we briefly review four quantum simulation experiments of Abelian lattice gauge theories based on ultracold atomic systems and then discuss recent developments towards experimentally friendly implementations.

Density-dependent gauge fields. A defining feature of lattice gauge theories is that the transport of matter is tied to interactions with the gauge field. Therefore, a first step towards the simulation of genuine lattice gauge theories consists of implementing a coupling mechanism between the gauge and matter fields, which reproduces this characteristic. In the experiment [26] ultracold fermions in an optical lattice were manipulated such that site-occupation-dependent Peierls phases mediated the hopping. Since the Peierls phase depends on the density this mechanism has been coined density-dependent gauge fields [79]. In order to realize such dynamics the Fermi–Hubbard Hamiltonian is driven with an inertial force $\hat{V}(\tau) = -f(\tau) \sum_{j,\sigma} \hat{n}_{j\sigma}$, where $f(t)$ is sinusoidally modulated at two frequencies and $\hat{n}_{j\sigma}$ is the density per site of a given hyperfine state σ . This Floquet scheme relies on breaking time-reversal symmetry by driving the lattice simultaneously at two frequencies resonant with the on-site interactions. For sufficiently fast driving, one obtains effective density-assisted tunnelling processes that are controllable in amplitude and phase. In the experiment [26], the authors characterized the tunnel coupling and detected two distinct regimes as a function of the modulation amplitudes which can be characterized by a \mathbb{Z}_2 -invariant.

Floquet engineering of a \mathbb{Z}_2 lattice gauge. The experimentalists of [25] also used the Floquet approach to realize a minimal instance of a \mathbb{Z}_2 lattice gauge theory. They achieved this by manipulating two components, $|a\rangle \equiv |F=1, m_F=-1\rangle$ and $|f\rangle \equiv |F=1, m_F=+1\rangle$, of ^{87}Rb in a double-well potential with a periodic drive. The double well potential was chosen species-dependent and allowed for both tunnel coupling between neighbouring sites and tuning of an energy offset. The energy offset was realized with a magnetic field gradient, making use of the magnetic moment of the Zeeman states. In particular, the offset is only experienced by the f -particles. In the limit of strong on-site interactions, the direct tunnelling processes are suppressed but can be restored through a periodic modulation at the resonance frequency. In the cases of resonant periodic driving, i.e. at the on-site interaction strength and judiciously chosen modulation parameters, the effective Floquet Hamiltonian turns into the desired two-site \mathbb{Z}_2 lattice gauge theory [80]. Here, matter and gauge fields are represented by two different species, corresponding to two Zeeman levels of the hyperfine groundstate manifold of ^{87}Rb . Matter fields are associated with a -states and the gauge field by the number imbalance of the f -states.

Local $U(1)$ symmetry from spin-changing collisions. In the experimental work [27], a scalable analogue quantum simulator of a $U(1)$ gauge theory was realized. Specifically, the experiment employed a mixture of two atomic Bose–Einstein condensates, ^{23}Na and ^7Li . The atoms in the two hyperfine states of sodium form an effective large spin representing the gauge fields, while the two hyperfine states of lithium correspond to two lattice sites of bosonic matter. The gauge invariant interactions between matter and gauge fields were engineered using inter-species spin changing collisions based on proposals of [81–84]. As an application, particle production from vacuum in the presence of a strong gauge field has been quantum-simulated.

Emergent local $U(1)$ symmetry for bosons in a superlattice The experiment [28] realized a large-scale quantum simulation of a $U(1)$ lattice gauge theory on 71 sites and has thus made a major step towards quantum simulation in the thermodynamic limit. A strongly tunable Bose–Hubbard

system, i.e. ultracold atoms in an optical superlattice, was employed. The gauge invariant interactions between matter and gauge field arise from a suitable choice of Hubbard parameters, which effectively suppresses unwanted processes via an energy penalty [19,85]. In the limit of strong interactions, this atomic system can then be rigorously mapped to a $U(1)$ lattice gauge theory with fermionic matter. The authors not only realized a $U(1)$ lattice gauge theory, but also quantified how well gauge invariance is satisfied in this quantum simulation. The Gauss Law has been evaluated by measurements of lattice site occupation and density-density correlations, which allow to quantify the local constraints imposed by gauge invariance. Furthermore, the large degree of tunability of this setup enabled a scan across a quantum phase transition.

(a) Challenges and new directions

These four experiments illustrate that the quantum simulation of Abelian lattice gauge theories with ultracold atom systems is a reality. Having passed this milestone, new experimental challenges are now being addressed. In particular, there is a continuing community effort in the following directions: (i) lattice gauge theories in higher dimensions [16,86], (ii) non-Abelian symmetries [20,21,87], (iii) lattice gauge theories with bosonic matter (see §2) and (iv) the effects of violating the local symmetries [88,89].

The quantum simulation of lattice gauge theories in higher dimensions has already achieved its first successes. For example, two-dimensional gauge theories have been realized in Rydberg arrays [90] or superconducting qubits [75]. Ultracold atom lattice experiments have realized a single ring-exchange interaction [91], but no large-scale quantum simulation yet. Another challenge is the quantum simulation of non-Abelian lattice gauge theories, where first attempts of digital simulations on universal quantum computers exist. However, the analogue quantum simulation of non-Abelian theories is still in its infancy. Many initial proposals for analogue quantum simulations of non-Abelian theories are beyond the current capabilities of ultracold atomic systems. Hence, there is great interest in experimentally feasible proposals for non-Abelian lattice gauge theories.

(i) Minimal $SU(2)$ models for ultracold atom systems

One outstanding challenge confronting the quantum simulation of non-Abelian lattice gauge theories is that one has to obey not one, but several non-commuting, local constraints [92]. However, instead of enforcing the local symmetry one can also eliminate the gauge fields or matter fields and quantum simulate the resulting reduced systems [93]. This encoding strategy was already successfully used for the first quantum simulation of the lattice Schwinger model with an ion quantum computer [24]. The encoding strategy can be applied for one-dimensional systems where the Gauss Law permits elimination of gauge degrees of freedom. Hence, one expects that this strategy can also work for non-Abelian lattice gauge theories. Moreover, the encoding approach can also be used for computational purposes, e.g. in the context of MPS [94]. In [95], the encoding strategy was used for two-site models to propose a quantum simulator of an $SU(2)$ lattice gauge theory and was mapped on a three- and four-level system. The four-level model can then be realized, e.g. with two coupled two-level systems like Rydberg atoms or coupling hyperfine states of atoms via microwave radiation. This mapping allows the study of certain minimal non-Abelian lattice gauge theories with current quantum simulator technology.

(ii) Non-Abelian gauge invariance from dynamical decoupling

Next we discuss a scalable strategy to quantum simulate non-Abelian lattice gauge theories. The earliest proposals for implementing non-Abelian lattice gauge theories with ultracold atom systems used atomic collisions [81], complex energy penalties [17,19] or elaborate digital schemes [96]. Another promising approach is the engineering of dissipation to enforce non-Abelian gauge invariance [97]. This dissipative approach is elegant since it requires a linear coupling to the Gauss

Law operators, but needs a correctly engineered dissipation. An immediate question is whether one can also enforce non-Abelian local symmetry through a coherent drive.

The question of enforcing global symmetries via coherent driving was previously addressed in the field of quantum information. In this context, the aim is to protect a target (sub)space for information processing. One strategy to minimize the interaction with the environment is dynamical decoupling [98]. In the first work [99], periodic bang-bang protocols were used to enforce global symmetries. In [100], the authors generalized this idea to a periodic bang-bang control to enforce a *local* symmetry. As a consequence the gauge invariant part of the Hilbert space decoupled from undesired sectors. The concept was demonstrated for a one-dimensional SU(2) lattice gauge system, but generalization to other non-Abelian symmetries and more dimensions is straightforward. A major advantage of the coherent driving approach is its generality. The application to ultracold atom systems is particularly appealing due to the local nature of typical gauge-violating processes, but the general scheme remains applicable for other platforms and thus opens a promising route for the quantum simulation of non-Abelian lattice gauge theories.

(iii) Rotor Jackiw–Rebbi model

Efforts towards simplifying the quantum simulation of lattice gauge theories also raise theoretical questions: which properties of lattice gauge theories are crucial to study high-energy systems or strongly correlated solids? Do simpler models without gauge invariance exhibit similar physics as gauge theories? To address these questions, the work [101] introduced a rotor-regularized version of the Jackiw–Rebbi model in (1+1)-dimensions. The original Jackiw–Rebbi quantum field theory [102] describes Dirac fermions interacting with a bosonic field. In contrast, the authors of [101] studied a regularized version of the Jackiw–Rebbi: fermions c_i on a lattice interacting with spins S_i on each lattice site. The regularized Hamiltonian is

$$H = \sum_i [-t(c_i^\dagger c_{i+1} + c_{i+1}^\dagger c_i) + \mathbf{g} \cdot \mathbf{S}_i c_i^\dagger c_i - \mathbf{h} \cdot \mathbf{S}_i]. \quad (5.1)$$

This model admits a simple implementation with an ultracold mixture in an optical lattice. Further, extensive numerical/analytical studies [101] revealed the spontaneous breaking of chiral symmetry [103], as well as a confinement-deconfinement transition. For a wide, experimentally relevant parameter regime, Dirac fermions acquire a dynamical mass via the spontaneous breakdown of chiral symmetry. At the confinement–deconfinement quantum phase transition meson-like bound states fractionalize into quark-like quasi-particles bound to topological solitons of the rotor field.

6. Conclusion and outlook

In this short essay, we have offered an overview of the rapidly developing research field of analogue quantum simulations for lattice gauge theory models. Since it is arduous to recapitulate the many significant achievements of the last decade in such a brief text, we have focused almost exclusively on contributions of collaborations involving the Quantum Optics Theory group at ICFO, with no intention of assessing their relevance against the work of others.

The most acknowledged goal of analogue quantum simulations is to create platforms for the embodiment of quantum many-body problems, which are both more tunable in their couplings and more accessible in their observables than their original counterparts in nature. This should ultimately serve to address open questions in a more decisive way than traditional computational techniques: something which often is dubbed as quantum supremacy, and that reflects the early vision of Feynman. In this respect, we are now contemplating an exciting explosion of experimental results that start to incarnate a decade of theoretical proposals. We are just starting to scratch an incredible world with a wealth of possibilities ahead. We could expect that also the first analogue quantum simulators of non-Abelian lattice gauge theories will, in another five

years or so, come to experimental birth. Such a step will be instrumental in embarking for the as yet unknown, e.g. exploring dynamical phenomena, or finite densities of matter, currently inaccessible to the best classical computational techniques. The first milestones in this respect have been set recently.

There is, however, still another prospect within reach of analogue quantum simulations, namely that of bringing abstract models into real laboratory life. By this we mean the realization of theoretical models that have been up to now only blackboard exercises, not directly observed in nature, as we have illustrated here in the case of bosonic matter. This will surely generate radically new phenomenology, which is not only exciting for pure curiosity-driven interests but could also eventually refertilize the field of condensed-matter, with possible technological outcomes on the long run. The intimate relation between these two big intellectual constructs, lattice gauge theory and condensed-matter physics, have indeed already shown its potential several times in the past.

Data accessibility. This article has no additional data.

Authors' contributions. All authors contributed to composition and edition of the paper. M. Lewenstein and J. Zakrzewski coordinated the section 'Introduction'. T. Chanda and L. Tagliacozzo coordinated the section 'Bosonic Schwinger Model'. D. González-Cuadra, with a help of A. Bermudez coordinated the section 'Strongly-correlated bosons on a dynamical lattice'. The section 'The synthetic Creutz-Hubbard model' was coordinated by E. Tirrito. The section 'Experimental and experimentally friendly quantum simulators' was led by V. Kasper, with a help of M. Aidelburger and F. Jendrzejewski. Finally, conclusions were coordinated by M. Rizzi.

Competing interests. We declare we have no competing interests.

Funding. The work of T.C. and J.Z. was realized within the QuantERA grant QTFLAG, financed by National Science Centre (Poland) via grant 2017/25/Z/ST2/03029. S.H. acknowledges support by STFC Consolidated Grant ST/T000813/1. L.T. acknowledges support from the Ramón y Cajal programme RYC-2016-20594, the 'Plan Nacional Generación de Conocimiento' PGC2018-095862-B-C22 and the State Agency for Research of the Spanish Ministry of Science and Innovation through the 'Unit of Excellence María de Maeztu 2020–2023' award to the Institute of Cosmos Sciences (CEX2019-000918-M). This project was supported by the European Union Regional Development Fund within the ERDF Operational Programme of Catalunya, Spain (project QUASICAT/QuantumCat, ref. 001- P-001644. E.Z. acknowledges the support of the Israel Science Foundation (grant no. 523/20). ICFO group acknowledges support from ERC AdG NOQIA, State Research Agency AEI ('Severo Ochoa' Center of Excellence CEX2019-000910-S) Plan National FIDEUA PID2019-106901GB-I00 project funded by MCIN/ AEI /10.13039/501100011033, FPI, QUANTERA MAQS PCI2019-111828-2 project funded by MCIN/AEI /10.13039/501100011033, Proyectos de I+D+I 'Retos Colaboración' RTC2019-007196-7 project funded by MCIN/AEI /10.13039/501100011033, Fundació Privada Cellex, Fundació Mir-Puig, Generalitat de Catalunya (AGAUR grant no. 2017 SGR 1341, CERCA programme, QuantumCAT U16-011424, co-funded by ERDF Operational Programme of Catalonia 2014-2020), EU Horizon 2020 FET-OPEN OPTOLogic (Grant No 899794), and the National Science Centre, Poland (symfonia grant no. 2016/20/W/ST4/00314), Marie Skłodowska-Curie grant STREDCH No 101029393, 'La Caixa' Junior Leaders fellowships (ID100010434), and EU Horizon 2020 under Marie Skłodowska-Curie grant agreement no. 847648 (LCF/BQ/PI19/11690013, LCF/BQ/PI20/11760031, LCF/BQ/PR20/11770012)).

Acknowledgements. We thank the referees of Philosophical Transactions of the Royal Society A for constructive and enriching suggestions. The TDVP simulations have been performed using ITensor library (<https://itensor.org>) and with a code based on a flexible Abelian Symmetric Tensor Networks Library, developed by the group of M. R. in collaboration with the group of S. Montangero (Padua). Support of PL Grid infrastructure is acknowledged. M.A. fur acknowledges funding from the European Research Council (ERC) under the European Union's Horizon 2020 research and innovation program (grant agreement no. 803047).

References

1. Trabesinger A. 2012 Quantum simulation. *Nat. Phys.* **8**, 263. (doi:10.1038/nphys2258)
2. Acín A *et al.* 2018 The quantum technologies roadmap: a European Community view. *New J. Phys.* **20**, 080201. (doi:10.1088/1367-2630/aad1ea)
3. Bernien H *et al.* 2017 Probing many-body dynamics on a 51-atom quantum simulator. *Nature* **551**, 579–584. (doi:10.1038/nature24622)
4. Tan WL *et al.* 2021 Domain-wall confinement and dynamics in a quantum simulator. *Nat. Phys.* **17**, 742–747. (doi:10.1038/s41567-021-01194-3)

5. Cirac JI, Zoller P. 2012 Goals and opportunities in quantum simulation. *Nat. Phys.* **8**, 264–266. (doi:10.1038/nphys2275)
6. Houck AA, Türeci HE, Koch J. 2012 On-chip quantum simulation with superconducting circuits. *Nat. Phys.* **8**, 292–299. (doi:10.1038/nphys2251)
7. Bloch I, Dalibard J, Nascimbène S. 2012 Quantum simulations with ultracold quantum gases. *Nat. Phys.* **8**, 267–276. (doi:10.1038/nphys2259)
8. Blatt R, Roos CF. 2012 Quantum simulations with trapped ions. *Nat. Phys.* **8**, 277–284. (doi:10.1038/nphys2252)
9. Celi A, Vermersch B, Viyuela O, Pichler H, Lukin MD, Zoller P. 2020 Emerging two-dimensional gauge theories in Rydberg configurable arrays. *Phys. Rev. X* **10**, 021057.
10. 2020 The ABC of cQED. *Nat. Phys.* **16**, 233–233. (doi:10.1038/s41567-020-0847-3)
11. Aspuru-Guzik A, Walther P. 2012 Photonic quantum simulators. *Nat. Phys.* **8**, 285–291. (doi:10.1038/nphys2253)
12. Dutta O, Gajda M, Hauke P, Lewenstein M, Lühmann D-S, Malomed BA, Sowiński T, Zakrzewski J. 2015 Non-standard Hubbard models in optical lattices: a review. *Rep. Prog. Phys.* **78**, 066001. (doi:10.1088/0034-4885/78/6/066001)
13. Abanin DA, Altman E, Bloch I, Serbyn M. 2019 Colloquium: many-body localization, thermalization, and entanglement. *Rev. Mod. Phys.* **91**, 021001. (doi:10.1103/RevModPhys.91.021001)
14. Büchler H, Hermele M, Huber S, Fisher MP, Zoller P. 2005 Atomic quantum simulator for lattice gauge theories and ring exchange models. *Phys. Rev. Lett.* **95**, 040402. (doi:10.1103/PhysRevLett.95.040402)
15. Osterloh K, Baig M, Santos L, Zoller P, Lewenstein M. 2005 Cold atoms in non-abelian gauge potentials: from the Hofstadter ‘moth’ to lattice gauge theory. *Phys. Rev. Lett.* **95**, 010403. (doi:10.1103/PhysRevLett.95.010403)
16. Wiese U-J. 2013 Ultracold quantum gases and lattice systems: quantum simulation of lattice gauge theories. *Ann. Phys.* **525**, 777–796. (doi:10.1002/andp.201300104)
17. Zohar E, Reznik B. 2011 Confinement and lattice quantum-electrodynamics electric flux tubes simulated with ultracold atoms. *Phys. Rev. Lett.* **107**, 275301. (doi:10.1103/PhysRevLett.107.275301)
18. Zohar E, Cirac JI, Reznik B. 2012 Simulating compact quantum electrodynamics with ultracold atoms: probing confinement and nonperturbative effects. *Phys. Rev. Lett.* **109**, 125302. (doi:10.1103/PhysRevLett.109.125302)
19. Banerjee D, Dalmonte M, Müller M, Rico E, Stebler P, Wiese U-J, Zoller P. 2012 Atomic quantum simulation of dynamical gauge fields coupled to fermionic matter: from string breaking to evolution after a quench. *Phys. Rev. Lett.* **109**, 175302. (doi:10.1103/PhysRevLett.109.175302)
20. Banerjee D, Bögli M, Dalmonte M, Rico E, Stebler P, Wiese U-J, Zoller P. 2013 Atomic quantum simulation of $U(N)$ and $SU(N)$ non-abelian lattice gauge theories. *Phys. Rev. Lett.* **110**, 125303. (doi:10.1103/PhysRevLett.110.125303)
21. Tagliacozzo L, Celi A, Orland P, Mitchell M, Lewenstein M. 2013 Simulation of non-abelian gauge theories with optical lattices. *Nat. Commun.* **4**, 2615. (doi:10.1038/ncomms3615)
22. Tagliacozzo L, Celi A, Zamora A, Lewenstein M. 2013 Optical Abelian lattice gauge theories. *Ann. Phys.* **330**, 160–191. (doi:10.1016/j.aop.2012.11.009)
23. Bañuls MC *et al.* 2020 Simulating lattice gauge theories within quantum technologies. *Eur. Phys. J. D* **74**, 165. (doi:10.1140/epjd/e2020-100571-8)
24. Martinez EA *et al.* 2016 Real-time dynamics of lattice gauge theories with a few-qubit quantum computer. *Nature* **534**, 516–519. (doi:10.1038/nature18318)
25. Schweizer C, Grusdt F, Berngruber M, Barbiero L, Demler E, Goldman N, Bloch I, Aidelsburger M. 2019 Floquet approach to Z_2 lattice gauge theories with ultracold atoms in optical lattices. *Nat. Phys.* **15**, 1168–1173. (doi:10.1038/s41567-019-0649-7)
26. Görg F, Sandholzer K, Minguzzi J, Desbuquois R, Messer M, Esslinger T. 2019 Realization of density-dependent Peierls phases to engineer quantized gauge fields coupled to ultracold matter. *Nat. Phys.* **15**, 1161–1167. (doi:10.1038/s41567-019-0615-4)
27. Mil A, Zache TV, Hegde A, Xia A, Bhatt RP, Oberthaler MK, Hauke P, Berges J, Jendrzejewski F. 2020 A scalable realization of local $U(1)$ gauge invariance in cold atomic mixtures. *Science* **367**, 1128–1130. (doi:10.1126/science.aaz5312)

28. Yang B, Sun H, Ott R, Wang H-Y, Zache TV, Halimeh JC, Yuan Z-S, Hauke P, Pan J-W. 2020 Observation of gauge invariance in a 71-site Bose–Hubbard quantum simulator. *Nature* **587**, 392–396. (doi:10.1038/s41586-020-2910-8)
29. Dutta O, Tagliacozzo L, Lewenstein M, Zakrzewski J. 2017 Toolbox for Abelian lattice gauge theories with synthetic matter. *Phys. Rev. A* **95**, 053608. (doi:10.1103/PhysRevA.95.053608)
30. Schwinger J. 1951 On gauge invariance and vacuum polarization. *Phys. Rev.* **82**, 664–679. (doi:10.1103/PhysRev.82.664)
31. Schwinger J. 1962 Gauge invariance and mass. *Phys. Rev.* **125**, 397–398. (doi:10.1103/PhysRev.125.397)
32. Coleman S. 1976 More about the massive Schwinger model. *Ann. Phys.* **101**, 239–267. (doi:10.1016/0003-4916(76)90280-3)
33. Hamer C, Kogut J, Crewther D, Mazzolini M. 1982 The massive Schwinger model on a lattice: background field, chiral symmetry and the string tension. *Nucl. Phys. B* **208**, 413–438. (doi:10.1016/0550-3213(82)90229-2)
34. Byrnes TMR, Sriganesh P, Bursill RJ, Hamer CJ. 2002 Density matrix renormalization group approach to the massive Schwinger model. *Phys. Rev. D* **66**, 013002. (doi:10.1103/PhysRevD.66.013002)
35. Bañuls M, Cichy K, Cirac J, Jansen K. 2013 The mass spectrum of the Schwinger model with matrix product states. *J. High Energy Phys.* **2013**, 158. (doi:10.1007/JHEP11(2013)158)
36. Buyens B, Haegeman J, Van Acoleyen K, Verschelde H, Verstraete F. 2014 Matrix product states for gauge field theories. *Phys. Rev. Lett.* **113**, 091601. (doi:10.1103/PhysRevLett.113.091601)
37. Chanda T, Zakrzewski J, Lewenstein M, Tagliacozzo L. 2020 Confinement and lack of thermalization after quenches in the bosonic Schwinger model. *Phys. Rev. Lett.* **124**, 180602. (doi:10.1103/PhysRevLett.124.180602)
38. Schöllwöck U. 2011 The density-matrix renormalization group in the age of matrix product states. *Ann. Phys.* **326**, 96–192. (doi:10.1016/j.aop.2010.09.012)
39. Paeckel S, Köhler T, Swoboda A, Manmana SR, Schollwöck U, Hubig C. 2019 Time-evolution methods for matrix-product states. *Ann. Phys.* **411**, 167998. (doi:10.1016/j.aop.2019.167998)
40. Ran S-J, Tirrito E, Peng C, Chen X, Tagliacozzo L, Su G, Lewenstein M. 2020 *Tensor network contractions : methods and applications to quantum many-body systems*. Lecture Notes in Physics vol. 964. Cham, Switzerland: Springer Nature.
41. Schuch N, Verstraete F, Cirac JI. 2004 Nonlocal resources in the presence of superselection rules. *Phys. Rev. Lett.* **92**, 087904. (doi:10.1103/PhysRevLett.92.087904)
42. Schuch N, Verstraete F, Cirac JI. 2004 Quantum entanglement theory in the presence of superselection rules. *Phys. Rev. A* **70**, 042310. (doi:10.1103/PhysRevA.70.042310)
43. Borla U, Verresen R, Grusdt F, Moroz S. 2020 Confined phases of one-dimensional spinless fermions coupled to Z_2 gauge theory. *Phys. Rev. Lett.* **124**, 120503. (doi:10.1103/PhysRevLett.124.120503)
44. Jaksch D, Bruder C, Cirac JI, Gardiner CW, Zoller P. 1998 Cold bosonic atoms in optical lattices. *Phys. Rev. Lett.* **81**, 3108–3111. (doi:10.1103/PhysRevLett.81.3108)
45. González-Cuadra D, Grzybowski PR, Dauphin A, Lewenstein M. 2018 Strongly correlated bosons on a dynamical lattice. *Phys. Rev. Lett.* **121**, 090402. (doi:10.1103/PhysRevLett.121.090402)
46. González-Cuadra D, Dauphin A, Grzybowski PR, Lewenstein M, Bermudez A. 2020 Dynamical solitons and boson fractionalization in cold-atom topological insulators. *Phys. Rev. Lett.* **125**, 265301. (doi:10.1103/PhysRevLett.125.265301)
47. Chanda T, González-Cuadra D, Lewenstein M, Tagliacozzo L, Zakrzewski J. 2020 Devil’s staircases of topological Peierls insulators and Peierls supersolids. (<https://arxiv.org/abs/2011.09228>)
48. González-Cuadra D, Dauphin A, Grzybowski PR, Wójcik P, Lewenstein M, Bermudez A. 2019 Symmetry-breaking topological insulators in the Z_2 Bose-Hubbard model. *Phys. Rev. B* **99**, 045139. (doi:10.1103/PhysRevB.99.045139)
49. González-Cuadra D, Dauphin A, Grzybowski PR, Lewenstein M, Bermudez A. 2020 Z_n solitons in intertwined topological phases. *Phys. Rev. B* **102**, 245137. (doi:10.1103/PhysRevB.102.245137)

50. Su WP, Schrieffer JR, Heeger AJ. 1979 Solitons in polyacetylene. *Phys. Rev. Lett.* **42**, 1698–1701. (doi:10.1103/PhysRevLett.42.1698)
51. Peierls R. 1955 *Quantum theory of solids*. International Series of Monographs on Physics. Oxford, UK: Clarendon Press.
52. Xiao D, Chang M-C, Niu Q. 2010 Berry phase effects on electronic properties. *Rev. Mod. Phys.* **82**, 1959–2007. (doi:10.1103/RevModPhys.82.1959)
53. González-Cuadra D, Bermudez A, Grzybowski PR, Lewenstein M, Dauphin A. 2019 Intertwined topological phases induced by emergent symmetry protection. *Nat. Commun.* **10**, 2694. (doi:10.1038/s41467-019-10796-8)
54. Thouless DJ. 1983 Quantization of particle transport. *Phys. Rev. B* **27**, 6083–6087. (doi:10.1103/PhysRevB.27.6083)
55. Bernevig BA. 2013 *Topological insulators and topological superconductors*. Princeton, NJ: Princeton University Press.
56. Wilson KG. 1977 New phenomena in subnuclear physics. *Erice Sch. Proc. Subnucl. Ser.* **13**, 13–32. (doi:10.1007/978-1-4613-4208-3_4)
57. Gatttringer C, Lang C. 2010 *Quantum chromodynamics on the lattice: an introductory presentation*, vol. 788. Lecture Notes Physics, vol. Berlin, Germany: Springer.
58. Bermudez A, Mazza L, Rizzi M, Goldman N, Lewenstein M, Martin-Delgado M. 2010 Wilson fermions and axion electrodynamics in optical lattices. *Phys. Rev. Lett.* **105**, 190404. (doi:10.1103/PhysRevLett.105.190404)
59. Mazza L, Bermudez A, Goldman N, Rizzi M, Martin-Delgado MA, Lewenstein M. 2012 An optical-lattice-based quantum simulator for relativistic field theories and topological insulators. *New J. Phys.* **14**, 015007. (doi:10.1088/1367-2630/14/1/015007)
60. Creutz M. 1999 End states, ladder compounds, and domain-wall fermions. *Phys. Rev. Lett.* **83**, 2636–2639. (doi:10.1103/PhysRevLett.83.2636)
61. Gross DJ, Neveu A. 1974 Dynamical symmetry breaking in asymptotically free field theories. *Phys. Rev. D* **10**, 3235–3253. (doi:10.1103/PhysRevD.10.3235)
62. Jünemann J, Piga A, Ran S-J, Lewenstein M, Rizzi M, Bermudez A. 2017 Exploring interacting topological insulators with ultracold atoms: the synthetic Creutz-Hubbard model. *Phys. Rev. X* **7**, 031057. (doi:10.1103/PhysRevX.7.031057)
63. Altland A, Zirnbauer MR. 1997 Nonstandard symmetry classes in mesoscopic normal-superconducting hybrid structures. *Phys. Rev. B* **55**, 1142–1161. (doi:10.1103/PhysRevB.55.1142)
64. Zak J. 1989 Berry's phase for energy bands in solids. *Phys. Rev. Lett.* **62**, 2747–2750. (doi:10.1103/PhysRevLett.62.2747)
65. Haller A, Matsoukas-Roubeas AS, Pan Y, Rizzi M, Burrello M. 2020 Exploring helical phases of matter in bosonic ladders. *Phys. Rev. Res.* **2**, 043433. (doi:10.1103/PhysRevResearch.2.043433)
66. Barbarino S, Rossini D, Rizzi M, Fazio R, Santoro GE, Dalmonte M. 2019 Topological devil's staircase in atomic two-leg ladders. *New J. Phys.* **21**, 043048. (doi:10.1088/1367-2630/ab0e18)
67. González-Cuadra D, Tagliacozzo L, Lewenstein M, Bermudez A. 2020 Robust topological order in fermionic F_2 gauge theories: from Aharonov-Bohm instability to soliton-induced deconfinement. *Phys. Rev. X* **10**, 041007. (doi:10.1103/PhysRevX.10.041007)
68. Ryu S, Schnyder AP, Furusaki A, Ludwig AW. 2010 Topological insulators and superconductors: tenfold way and dimensional hierarchy. *New J. Phys.* **12**, 065010. (doi:10.1088/1367-2630/12/6/065010)
69. Tirrito E, Rizzi M, Sierra G, Lewenstein M, Bermudez A. 2019 Renormalization group flows for Wilson-Hubbard matter and the topological Hamiltonian. *Phys. Rev. B* **99**, 125106. (doi:10.1103/PhysRevB.99.125106)
70. Bermudez A, Tirrito E, Rizzi M, Lewenstein M, Hands S. 2018 Gross-Neveu-Wilson model and correlated symmetry-protected topological phases. *Ann. Phys.* **399**, 149–180. (doi:10.1016/j.aop.2018.10.007)
71. Ziegler L, Tirrito E, Lewenstein M, Hands S, Bermudez A. 2020 Correlated Chern insulators in two-dimensional Raman lattices: a cold-atom regularization of strongly-coupled four-fermi field theories. (<https://arxiv.org/abs/2011.08744>)

72. Qi X-L, Wu Y-S, Zhang S-C. 2006 Topological quantization of the spin hall effect in two-dimensional paramagnetic semiconductors. *Phys. Rev. B* **74**, 085308. (doi:10.1103/PhysRevB.74.085308)
73. Haldane FDM. 1988 Model for a quantum hall effect without Landau levels: condensed-matter realization of the 'parity anomaly'. *Phys. Rev. Lett.* **61**, 2015–2018. (doi:10.1103/PhysRevLett.61.2015)
74. Kokail C *et al.* 2019 Self-verifying variational quantum simulation of lattice models. *Nature* **569**, 355–360. (doi:10.1038/s41586-019-1177-4)
75. Satzinger K *et al.* 2021 Realizing topologically ordered states on a quantum processor. (<https://arxiv.org/abs/2104.01180>)
76. Endres M *et al.* 2011 Observation of correlated particle-hole pairs and string order in low-dimensional mott insulators. *Science* **334**, 200–203. (doi:10.1126/science.1209284)
77. Schweigler T *et al.* 2017 Experimental characterization of a quantum many-body system via higher-order correlations. *Nature* **545**, 323–326. (doi:10.1038/nature22310)
78. Islam R, Ma R, Preiss PM, Eric Tai M, Lukin A, Rispoli M, Greiner M. 2015 Measuring entanglement entropy in a quantum many-body system. *Nature* **528**, 77–83. (doi:10.1038/nature15750)
79. Greschner S, Sun G, Poletti D, Santos L. 2014 Density-dependent synthetic gauge fields using periodically modulated interactions. *Phys. Rev. Lett.* **113**, 215303. (doi:10.1103/PhysRevLett.113.215303)
80. Barbiero L, Schweizer C, Aidelsburger M, Demler E, Goldman N, Grusdt F. 2019 Coupling ultracold matter to dynamical gauge fields in optical lattices: from flux attachment to Z_2 lattice gauge theories. *Sci. Adv.* **5**, eaav7444. (doi:10.1126/sciadv.aav7444)
81. Zohar E, Cirac JI, Reznik B. 2013 Quantum simulations of gauge theories with ultracold atoms: local gauge invariance from angular-momentum conservation. *Phys. Rev. A* **88**, 023617. (doi:10.1103/PhysRevA.88.023617)
82. Kasper V, Hebenstreit F, Oberthaler M, Berges J. 2016 Schwinger pair production with ultracold atoms. *Phys. Lett. B* **760**, 742–746. (doi:10.1016/j.physletb.2016.07.036)
83. Kasper V, Hebenstreit F, Jendrzejewski F, Oberthaler MK, Berges J. 2017 Implementing quantum electrodynamics with ultracold atomic systems. *New J. Phys.* **19**, 023030. (doi:10.1088/1367-2630/aa54e0)
84. Zache TV, Hebenstreit F, Jendrzejewski F, Oberthaler M, Berges J, Hauke P. 2018 Quantum simulation of lattice gauge theories using Wilson fermions. *Quantum Sci. Technol.* **3**, 034010. (doi:10.1088/2058-9565/aac33b)
85. Fradkin E. 2013 *Field theories of condensed matter physics*. Cambridge, UK: Cambridge University Press.
86. Zohar E, Cirac JI, Reznik B. 2015 Quantum simulations of lattice gauge theories using ultracold atoms in optical lattices. *Rep. Prog. Phys.* **79**, 014401. (doi:10.1088/0034-4885/79/1/014401)
87. Zohar E, Cirac JI, Reznik B. 2013 Cold-atom quantum simulator for SU(2) yang-mills lattice gauge theory. *Phys. Rev. Lett.* **110**, 125304. (doi:10.1103/PhysRevLett.110.125304)
88. Halimeh JC, Hauke P. 2020 Reliability of lattice gauge theories. *Phys. Rev. Lett.* **125**, 030503. (doi:10.1103/PhysRevLett.125.030503)
89. Halimeh JC, Kasper V, Hauke P. 2020 Fate of lattice gauge theories under decoherence. (<https://arxiv.org/abs/2009.07848>)
90. Semeghini G *et al.* 2021 Probing topological spin liquids on a programmable quantum simulator. (<https://arxiv.org/abs/2104.04119>)
91. Dai H-N, Yang B, Reingruber A, Sun H, Xu X-F, Chen Y-A, Yuan Z-S, Pan J-W. 2017 Four-body ring-exchange interactions and anyonic statistics within a minimal toric-code Hamiltonian. *Nat. Phys.* **13**, 1195–1200. (doi:10.1038/nphys4243)
92. Kogut J, Susskind L. 1975 Hamiltonian formulation of Wilson's lattice gauge theories. *Phys. Rev. D* **11**, 395–408. (doi:10.1103/PhysRevD.11.395)
93. Muschik C *et al.* 2017 U(1) Wilson lattice gauge theories in digital quantum simulators. *New J. Phys.* **19**, 103020. (doi:10.1088/1367-2630/aa89ab)
94. Bañuls MC, Cichy K, Ignacio Cirac J, Jansen K, Kühn S. 2017 Efficient basis formulation for $(1 + 1)$ -dimensional SU(2) lattice gauge theory: spectral calculations with matrix product states. *Phys. Rev. X* **7**, 041046.

95. Kasper V, Juzeliunas G, Lewenstein M, Jendrzejewski F, Zohar E. 2020 From the Jaynes-Cummings model to non-abelian gauge theories: a guided tour for the quantum engineer. *New J. Phys.* **22**, 103027. (doi:10.1088/1367-2630/abb961)
96. Zohar E, Farace A, Reznik B, Cirac JL. 2017 Digital quantum simulation of Z_2 lattice gauge theories with dynamical fermionic matter. *Phys. Rev. Lett.* **118**, 070501. (doi:10.1103/PhysRevLett.118.070501)
97. Stannigel K, Hauke P, Marcos D, Hafezi M, Diehl S, Dalmonte M, Zoller P. 2014 Constrained dynamics via the Zeno effect in quantum simulation: implementing non-abelian lattice gauge theories with cold atoms. *Phys. Rev. Lett.* **112**, 120406. (doi:10.1103/PhysRevLett.112.120406)
98. Lidar DADA, Brun TA, Alicki R. 2013 *Quantum error correction*. Cambridge, England: Cambridge University Press.
99. Viola L, Knill E, Lloyd S. 1999 Dynamical decoupling of open quantum systems. *Phys. Rev. Lett.* **82**, 2417–2421. (doi:10.1103/PhysRevLett.82.2417)
100. Kasper V, Zache TV, Jendrzejewski F, Lewenstein M, Zohar E. 2020 Non-Abelian gauge invariance from dynamical decoupling. (<https://arxiv.org/abs/2012.08620>)
101. González-Cuadra D, Dauphin A, Aidelsburger M, Lewenstein M, Bermudez A. 2020 Rotor Jackiw-Rebbi model: a cold-atom approach to chiral symmetry restoration and charge confinement. *PRX Quantum* **1**, 20321. (doi:10.1103/PRXQuantum.1.020321)
102. Jackiw R, Rebbi C. 1976 Solitons with fermion number $1/2$. *Phys. Rev. D* **13**, 3398–3409. (doi:10.1103/PhysRevD.13.3398)
103. Nambu Y, Jona-Lasinio G. 1961 Dynamical model of elementary particles based on an analogy with superconductivity. I. *Phys. Rev.* **122**, 345–358. (doi:10.1103/PhysRev.122.345)